Near-Field Two-Photon-Induced Photoluminescence from Single Gold Nanorods and Imaging of Plasmon Modes

Kohei Imura,[†,‡] Tetsuhiko Nagahara,[†] and Hiromi Okamoto*[,†,‡]

Institute for Molecular Science, Okazaki 444-8585, Japan, and The Graduate University for Advanced Studies, Okazaki 444-8585, Japan

Received: March 30, 2005; In Final Form: May 9, 2005

We investigated the two-photon-induced photoluminescence properties of single gold nanorods by scanning near-field spectroscopy. The process was found to be initiated by a sequential one-photon absorption for creating a pair of an electron and a hole in the sp and d bands. Photoluminescence is then radiated when the electron near the Fermi surface recombines with the hole near the *X* and *L* symmetry points. The polarization characteristics of emitted photons from the *X* and *L* regions were found to be different. These characteristics can be understood by the crystalline structure and the band structure of the gold nanorod. We found characteristic spatial oscillatory features along the long axis of the nanorods in photoluminescence excitation images. The images were well reproduced by density-of-states maps of the nanorods calculated with Green's dyadic method and were attributed to the spatial characteristics of the wave functions of the plasmon modes inside the nanorods.

Introduction

Surface plasmon resonance (SPR) of noble metals has attracted much interest, since SPR is of fundamental importance not only in science but also in various applications in nanotechnology.[1] It is known that the SPR can be an origin of strong electric-field enhancement due to the electric-field confinement on the nanometric scale. When molecules are adsorbed on junctions of the noble metal particles or on roughened noble metallic films, a huge field enhancement occurs. The enhancement gives rise to giant surface enhanced Raman scattering (SERS) signals of molecules.[2,3] For the roughened metallic film system, it has been frequently reported that a spectrally broad background photoluminescence (PL) is observed in addition to the sharp SERS signal.[3] These observations caused interest in PL from noble metals. Boyed et al.[4] investigated PL from the metallic films and assigned the origin of the PL to radiative recombination of excited electrons near the Fermi surface in the sp conduction band with holes in the d band.

On the other hand, studies of PL from the metal nanoparticles were limited because of very low quantum efficiencies.[5] A strong enhancement of PL from gold nanorods upon single photon excitation was reported.[6] The enhancement was ascribed to the local field enhancement due to the SPR of the gold nanorods. Two-photon optical processes involve an additional field enhancement, and thus, a greater enhancement of PL efficiency is expected in comparison with the one-photon case. In fact, we found that a two-photon process can effectively excite PL.[7] It was also found that two-photon-induced PL (TPI-PL) is useful for revealing the spatial characteristics of the plasmon modes (square moduli of plasmon wave functions) in gold nanorods. Knowledge of the spatial characteristics of the plasmons, as well as the spectral and polarization characteristics, is essential for control of electric-field confinement in the near-field and of plasmon properties.

In this paper, we investigate TPI-PL from single gold nanorods of a variety of lengths and diameters using an apertured scanning near-field optical microscope (SNOM), to characterize the emission mechanism and the optical features of the TPI-PL process. The spatial characteristics of the plasmon modes are also studied. We analyze the relationships between the crystalline structure and the polarization characteristics of the TPI-PL. We also discuss the importance of the local plasmon mode excitation in the emission process and in creating a strong field enhancement inside the gold nanorods.

Experimental Section

Gold nanorods were synthesized chemically in solutions by a seed-mediated method following the report by Busbee et al.[8] Chemicals were purchased from Wako Pure Chemicals and used as received. To separate the gold nanorods from spherical products, the sample solution was centrifuged at 1500 rpm for 20 min; the supernatant was then poured off and water was added to the precipitate to redisperse it. This process was repeated several times so that surfactant molecules were taken away from the sample solution. The morphologies of the gold nanorods were verified by topography measurements by a SNOM apparatus and/or by a scanning electron microscope (SEM) (Hitachi, S-900). Figure 1 shows a SEM image of the synthesized gold nanorods. The diameter and aspect ratio of the gold nanorods range from 15 to 40 nm and from 2 to more than 50, respectively. For SNOM measurements, gold nanorods were spin-coated on coverslips.

An apertured type SNOM was operated under ambient conditions. Either aluminum- or gold-coated apertured near-field optical fiber probes (JASCO Corp.) were used. The diameters of the probe aperture were measured by a SEM image of the tip or by near-field fluorescence excitation images of single molecules. The typical diameter of the aperture was 50−100 nm. A shear-force feedback method was utilized to maintain the near-field probe in the vicinity of the sample surface, and its feedback signal was used to construct a topographic image.

* To whom correspondence should be addressed. E-mail: aho@ims.ac.jp.
† Institute for Molecular Science.
‡ The Graduate University for Advanced Studies.

10.1021/jp051631o CCC: $30.25
Published on Web 06/16/2005

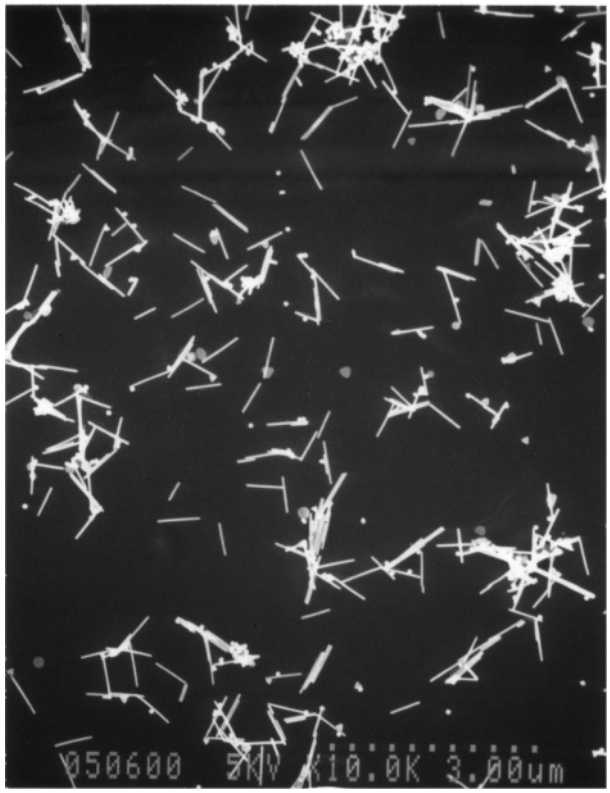

Figure 1. Scanning electron micrograph of gold nanorods.

A Ti:sapphire laser (Spectra-Physics, $\lambda = 780-840$ nm, <100 fs, 80 MHz) was used for exciting the TPI-PL, and its output was coupled to the other end of the near-field fiber probe.[7] Single gold nanorods were illuminated locally from the aperture of the near-field probe. Emitted PL was collected by an objective (Nikon, NA = 0.8) and directed to a detection system. To suppress interference by the excitation laser and by stray light, a notch filter and other appropriate filters were used. A polychromator−CCD system was used for PL spectral measurements, and an avalanche photodiode (Perkin-Elmer, SPCM-AQR-14) was used for time-correlated single-photon-counting (TCSPC), imaging, and polarization measurements. The TCSPC measurements were performed to gain dynamical information on the TPI-PL process. For the TCSPC measurements, output pulses from the avalanche photodiode were treated by a time-to-amplitude converter (EG&G, TAC566) and a multichannel buffer (EG&G, MCB921). An instrument response function had a full width at half-maximum (fwhm) of about 350 ps, which was limited by the time response of the avalanche photodiode.

For effective excitation of the TPI-PL, short pulses at the near-field tip are essential. To keep the pulse duration short at the tip, group velocity dispersion for the incident light arising from the optical fiber was precompensated. To characterize the pulse duration at the near-field tip, we used an autocorrelation measurement of either a two-photon-induced photocurrent in a GaAsP photodiode (Hamamatsu, G1117)[9] or a second harmonic generation (SHG) in a single gold particle. For a SHG intensity measurement, a photomultiplier tube (Hamamatsu, R636-10 or R2969) was used. The typical pulse duration was found to be ~100 fs (fwhm).

To characterize the detailed PL property in relation to the crystalline structures of the gold nanorods, we performed polarization dependence measurements with a SNOM. We measured the PL intensity as a function of the polarization direction of the excitation photons, that of the emitted photons, and the excitation wavelength. The excitation polarization of the light from the tip was controlled by a quarter- and a half-wave plate placed before the fiber coupler. The purity of the linear polarization from the near-field tip was from 20:1 to 8:1, as determined in the far-field. A sheet polarizer was placed before the detector and used to analyze the polarization characteristics of the emitted PL by adjusting the polarizer angle with respect to the nanorods.

Local-Density-of-States (LDOS) Calculation

To analyze the observed optical images of nanorods, we calculate the electromagnetic LDOS around the nanorod by using Green's dyadic method.[10−12] The LDOS at a position, $\vec{r}$, for an optical angular frequency, ω, $\rho(\vec{r},\omega)$, is defined by a complete set of orthonormal eigenfunctions, $\phi_n(\vec{r})$

$$\rho(\vec{r},\omega) = \sum_n \delta(\omega - \omega_n)\phi_n(\vec{r})\,\phi_n^*(\vec{r}) \qquad (1)$$

where ω_n represents the nth electromagnetic eigenfrequency of the plasmon mode. Hence, near the resonance frequency, ω_n, the LDOS is approximately equivalent to the square modulus of an eigenfunction associated with the nth electromagnetic eigenmode.

The Green dyadic, $\overleftrightarrow{G}(\vec{r},\vec{r}',\omega)$, is defined as the solution of eq 2

$$-\nabla \times \nabla \times \overleftrightarrow{G}(\vec{r},\vec{r}',\omega) + k_0^2\epsilon_0(\vec{r})\overleftrightarrow{G}(\vec{r},\vec{r}',\omega) + k_0^2\epsilon_s(\vec{r}',\omega)\overleftrightarrow{G}(\vec{r},\vec{r}',\omega) = \delta(\vec{r} - \vec{r}') \qquad (2)$$

where k_0 is the absolute value of the wave vector of light in a vacuum and ϵ_0 and ϵ_s represent the dielectric constants for the homogeneous reference system and for the scattering object, respectively. The LDOS can be extracted from the Green dyadic using the relation[10,12]

$$\rho(\vec{r},\omega) = -\frac{1}{\pi}\mathrm{tr}[\mathrm{Im}\{\overleftrightarrow{G}(\vec{r},\vec{r},\omega)\}] \qquad (3)$$

where tr and Im stand for the trace and imaginary part of $\overleftrightarrow{G}(\vec{r},\vec{r},\omega)$, respectively. The Green dyadic, $\overleftrightarrow{G}(\vec{r},\vec{r}',\omega)$, of the entire scattering system can be numerically solved by the self-consistent discretized Dyson equation starting from the analytically known Green dyadic of the homogeneous medium,[13] $\overleftrightarrow{G}_0(\vec{r},\vec{r}',\omega)$, as follows:

$$\overleftrightarrow{G}(\vec{r},\vec{r}',\omega) = \overleftrightarrow{G}_0(\vec{r},\vec{r}',\omega) + \overleftrightarrow{G}_0(\vec{r},\vec{r}',\omega)k_0^2[\epsilon_0(\vec{r}) - \epsilon_s(\vec{r}',\omega)]\overleftrightarrow{G}(\vec{r},\vec{r}',\omega) \qquad (4)$$

In the present calculation, a cylindrical mesh was adopted, and the depolarizing effect in the source region (renormalization procedure) was also taken into account.[14] In this way, electromagnetic boundary conditions are automatically satisfied.

Results and Discussion

A. Mechanism of the PL from Single Gold Nanorods. Figure 2 shows a typical TPI-PL spectrum measured for a single gold nanorod excited at a wavelength of 780 nm. Two peaks are clearly seen in the figure. Provided that the PL mechanism for gold nanorods is essentially the same as that for metallic films,[4] the peak energy of the emitted photons should be given by the energy separation between the Fermi surface and the holes in the d band. In gold crystals, it is expected that optical transitions preferentially occur near the X and L symmetry points

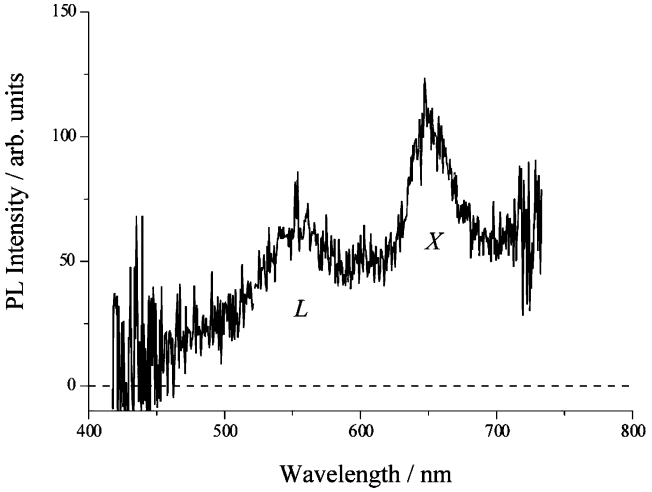

Figure 2. Two-photon-induced photoluminescence (TPI-PL) spectrum from a single gold nanorod. The dashed line shows a baseline at the bare substrate.

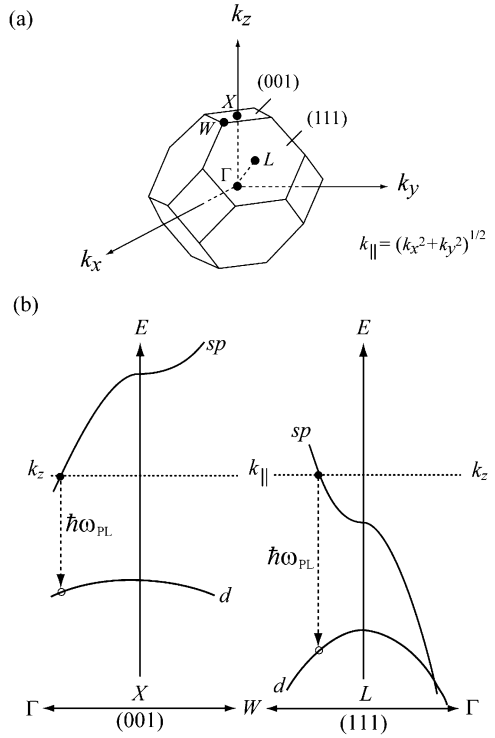

Figure 3. (a) Symmetry points and symmetry axes in the first Brillouin zone of gold. (b) Schematic diagrams of band structures near the *X* and *L* symmetry points. $\hbar\omega_{PL}$ denotes the photon energy of the PL, radiated by filling a hole with an electron from the sp band. The notations sp and d denote the sp conduction band and the d band, respectively. The dashed lines indicate the Fermi surfaces.

of the Brillouin zone, since the density-of-states near these symmetry points are high. Band structures near the *X* and *L* symmetry points are shown in Figure 3b. According to the calculated band structures of gold,[15] emission peaks should be observed around wavelengths of 630 and 520 nm, respectively, for the regions of the *X* and *L* symmetry points. Two peaks observed in Figure 2 (around 650 and 550 nm) appear very close to this expectation and thus are assigned to the PL arising from the electron−hole recombination near the *X* and *L* symmetry points, respectively. Details of the spectral features are discussed later.

Dynamic measurements give information on the properties of the excited states. We have examined the PL decay of various

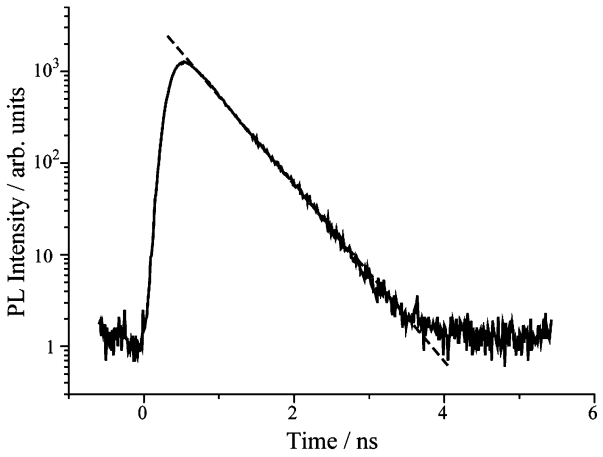

Figure 4. Typical time-correlated single-photon-counting (TCSPC) profile of the TPI-PL. The excitation and detection wavelengths are 780 and 550 ± 10 nm, respectively. The dashed line shows a least-squares fit.

gold particles at various emission wavelengths by the TCSPC measurements. Figure 4 shows a typical result. The observed decay was fitted to a single exponential function, and the lifetime was determined to be ~1.0 ns. We have found that the lifetime depends on the size and shape of the particles and also on the detection wavelength, and it ranges from 0.8 to 2 ns. One may notice that the lifetime is quite long compared to those found in ultrafast pump−probe measurements of gold nanoparticles, where the lifetimes of the excited electrons were found to be less than several picoseconds.[16−20] Recently, time-resolved fluorescence upconversion experiments were performed to measure the lifetime of the PL.[21,22] In the upconversion trace, a very slow component was found which did not decay within the measured time range (3 ps), in addition to an ultrafast component on a time scale of 50 fs.[22] The slow component may be attributed to the same relaxation process as that found in the present study. Fermi liquid theory predicts that the lifetime of the excited electron quadratically decreases with the difference between the energy of the excited electron and the Fermi level.[23] In fact, a time-resolved two-photon photoemission study confirmed this prediction experimentally.[24] The long lifetime of the PL observed here might indicate that the PL is effectively radiated by the recombination of excited electrons located very close to the Fermi surface with holes in the d band. This idea is inconsistent with the proposed PL mechanism described above.

B. Polarization Characteristics. We have investigated dependencies of the PL intensity on the polarizations of both the excitation (incoming) and emitted (outgoing) photons, as shown in Figure 5. Uncertainty of the absolute polarization angle, θ, is ±10°. The dependence of the PL intensity on the incident electric-field polarization (Figure 5a) indicates that the polarized field along the long axis of the nanorod can predominantly excite the PL. It follows a $\cos^2\theta$ dependence. For two-photon excitation processes, two different schemes can be considered: a sequence of one-photon excitations and a coherent two-photon excitation. These two cases are distinguished by different behavior on the incident polarizations. SHG is known as a coherent process. In this case, the SHG intensity is expected to follow a $\cos^4\theta$ dependence against the incident polarization. We measured the SHG from a single gold nanorod, and the incident polarization dependence is shown in Figure 5b. It shows a clear $\cos^4\theta$ dependence as expected. The different polarization characteristics between TPI-PL and SHG are thus trustworthy,

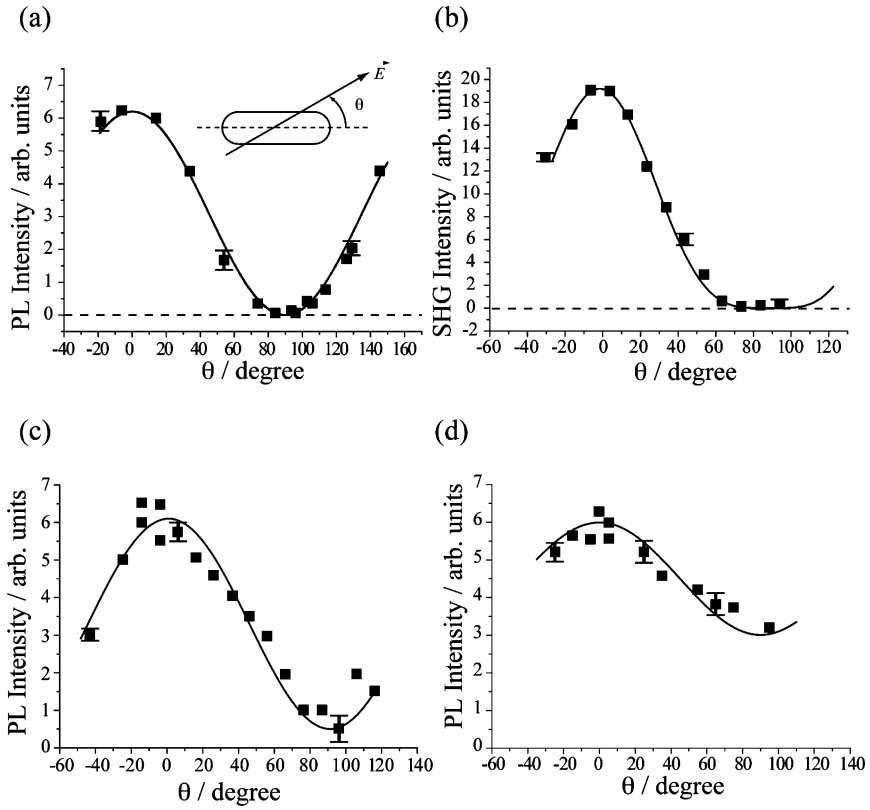

Figure 5. (a) Incident light polarization dependence of the PL intensity, where emitted photons ranging from 450 to 650 nm in wavelength were detected without specifying the polarization. The solid curve shows a $\cos^2 \theta$ function. (b) Incident polarization dependence of the SHG intensity. The SHG was measured near 390 nm in wavelength without specifying the polarization. The solid curve shows a $\cos^4 \theta$ function. (c) Polarization characteristics of the detected photons of the PL measured at the center of the *X* region (645−655 nm), where the incident field was polarized parallel to the long axis of the nanorod. The solid curve shows a $\cos^2 \theta$ function. (d) Polarization characteristics of the detected photons of the PL measured near the *L* region (450−550 nm), where the incident field was polarized parallel to the long axis of the nanorod. The solid curve shows a $\cos^2 \theta$ function.

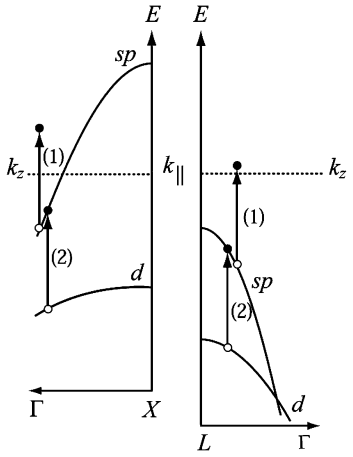

Figure 6. Excitation schemes of sequential one-photon absorptions near the *X* and *L* symmetry points. Open and closed circles denote holes and electrons, respectively.

and the $\cos^2 \theta$ dependence of the TPI-PL is attributed to the sequential one-photon process.

As discussed in the previous subsection, PL is radiated when the electrons near the Fermi surface (on the sp band) and the holes in the d band recombine. It has been revealed from the discussion above that electron−hole pairs are created in these bands by the sequential one-photon process. The excitation mechanism can be hence described as follows (Figure 6). Upon the optical excitation, the first photon excites an electron in the sp conduction band located below the Fermi surface to the sp conduction band above the Fermi surface via an intraband transition. At the same time, a hole is created in the sp conduction band below the Fermi level. This transition is resonant with photons with a polarization along the long axis of the nanorod. After the excitation, the memory of the polarization is rapidly lost. Then, the second photon excites an electron in the d band to the sp conduction band, where the hole was created by the first photon. The transition by the second photon is not sensitive to the polarization. The second photon generates a hole in the d band. As a consequence, an electron−hole pair is generated, which can recombine to radiate later.

Parts c and d of Figure 5 show the polarization characteristics of the emitted photons from the *X* (645−655 nm) and *L* (450−550 nm) regions, respectively. The emission from the *X* region shows an almost perfect polarization along the long axis of the rod with a $\cos^2 \theta$ intensity dependence on the angle θ, while that from the *L* region exhibits only a partially polarized PL. The incident field is polarized along the long axis of the rod in the measurements of Figure 5c and d. However, the polarization characteristics of the emitted photons were independent of the incident polarization. These characteristics are understood as follows on the basis of the crystalline structures of the gold nanorods.

Structural information on gold nanorods was reported by electron-beam diffraction studies and high-resolution transmission electron microscopy (HR-TEM).[25−27] It has been established that the chemically synthesized gold nanorod is a single crystal. Dominant side facets are (110), and the growth direction is [001]. The ends of the nanorods are (001) and (111) facets of small areas, as shown in Figure 7. According to atomic-dipole selection rules,[28−30] allowed transitions of the recombination

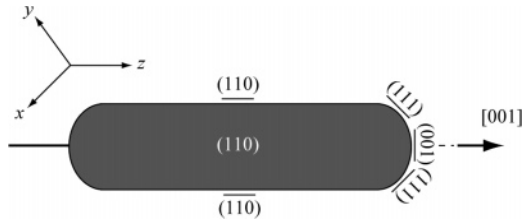

Figure 7. Schematic structure of the gold nanorod.

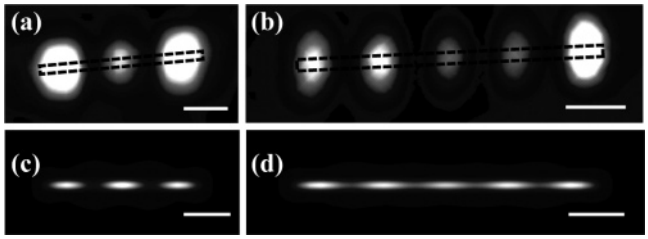

Figure 8. TPI-PL images for single gold nanorods: (a) 20 ± 5 nm $\times$ 330 ± 30 nm; (b) 20 ± 5 nm $\times$ 540 ± 40 nm. (c and d) Calculated LDOS maps for the corresponding gold nanorods (a and b), respectively. The scale bars are 100 nm.

TABLE 1: Allowed Transitions in the *X* and *L* Regions

symmetry point	direction of the transition moment
X	parallel to the *xy*, *yz*, or *zx* planes
L	parallel to the (111) planes

emission in the *X* and *L* regions are restricted to certain directions, as summarized in Table 1, where the directions of *x*, *y*, and *z* are defined in Figure 7. In the case of the transition in the *X* region, the transition moment can take any direction in the *yz*, *zx*, or *xy* plane (i.e., the moment is perpendicular to one or more of the *x*, *y*, or *z* axes). From this dipole selection rule, unpolarized PL could be expected. However, experimental observation shows, on the contrary, an almost perfect polarization with $\cos^2 \theta$ dependence for the PL in the *X* region (Figure 5c). We should notice that the direction of the allowed transition can be parallel to any axis of the nanorod (*x*, *y*, or *z*). The observed results in Figure 5c imply that the electronic oscillation along the long axis (*z*) of the rod is resonantly coupled strongly to the PL, to give the *z*-polarized PL. On the other hand, in the case of the transition in the *L* region, the transition moment is parallel to (111) planes. The (111) planes are not parallel to any axis of the nanorod, as can be seen in Figure 7, so that the electric vectors of the emitted photons cannot be parallel to the [001] (*z*) direction. As a result, PL from the *L* region is partially polarized. In Figure 5d, the PL is enhanced at $\theta \sim 0°$ rather than at $\theta \sim 90°$. This observation suggests that the PL transition polarized along directions close to the long axis is enhanced, compared to that with a polarization perpendicular to the axis. In this way, the polarization characteristics obtained can be reasonably understood on the basis of the crystalline structure and the band structure of the gold nanorods. It is also to be noted that PL excited at any position on the rod shows identical polarization dependences. This finding is again consistent with the single crystal nature of the gold nanorod.

C. Spatial Characteristics of Plasmon Modes. By monitoring the TPI-PL from single nanorods, it is possible to image the spatial characteristics of plasmon modes. Figure 8a and b shows two typical near-field TPI-PL images observed for single gold nanorods, where the incident field was parallel to the rod axis. PL in the range between 450 and 650 nm was detected in both cases. The dotted squares indicate the approximate shapes of the rods estimated from the topographic measurements. The estimated rod dimensions (diameter $\times$ length) are 20 ± 5 nm $\times$ 330 ± 40 nm for part a and 20 ± 5 nm $\times$ 540 ± 60 nm for part b. The PL can only be excited when the distance from the rod surface to the near-field probe tip is less than $\sim$50 nm. In Figure 8, we should note the following point. An apertured SNOM can locally excite the TPI-PL at a specific position on the nanorod. However, the excitation energy may rapidly propagate along the nanorod before emitting the PL.[31] Since the total emission from the nanorod was detected (not that from a specific point of the rod), the measured PL intensity gives the excitation probability of the TPI-PL at the tip position, not a spatial distribution of the emission.

As can be seen in the figure, the PL intensities show characteristic spatial oscillations along the long axis. The separation between the bright parts of the oscillating patterns is $\sim$100$-$150 nm. The oscillatory structures found in Figure 8a and b represent the spatial characteristics of the plasmon modes (square moduli of the plasmon wave functions, as is similar to those found for excitons in semiconductor quantum dots[32]) of the nanorods at the excitation wavelength. Figure 8c and d shows calculated LDOS images for the corresponding nanorods. The good agreement between the observations and the calculated LDOS images supports the idea mentioned above, since the LDOS is defined as a sum of square moduli of wave functions (eq 1). We have measured TPI-PL images for more than 100 nanorods and have found similar oscillating patterns along the long axis of nanorods. We have found that the number of oscillations increases with the increment of aspect ratio. The results show a good correspondence to the finding of a single dispersion relation of SP modes, for the nanorods of various lengths with a fixed diameter, in near-field transmission measurements.[33]

Now, we discuss local field enhancements due to the motion of free electrons, which determine the spatial patterns of the TPI-PL images in Figure 8. The origin of enhancements is divided into two factors, the "lightning rod effect" (at a sharp angled surface) and shape dependent effects due to resonant localized plasmon modes. The lightning rod effect is basically wavelength independent, while the resonant plasmon effects are strongly wavelength dependent. If the former effect is dominant, the enhancement should occur predominantly at end-edge parts of the nanorods. Then, the TPI-PL image should give bright spots at the end edges. In fact, some nanorods emit the PL upon exciting the edge parts.[7] As for the results shown in Figure 8, the enhancement is not localized in the edges, and the excitation probability of the TPI-PL is explained primarily by the effect due to the resonant plasmon mode.

To confirm that, we examined an excitation wavelength dependence of the PL intensity for a single gold nanorod (25 ± 5 nm $\times$ 520 ± 50 nm). In this measurement, the incident field was polarized parallel to the long axis of the nanorod, and the PL ranging from 450 to 650 nm was detected. As shown in Figure 9, a prominent incident wavelength dependence was found. The result supports the idea that the primary factor for the clear spatial oscillating pattern found in the TPI-PL images is the excitation of local plasmon resonances.

D. Intensity Enhancements Induced by Local Plasmons and the Spectral Features of the PL. As discussed in the previous subsection, the electric-field enhancement due to the plasmon mode resonance is one of the important factors for observing TPI-PL. In this subsection, we conduct the electric-field calculation by the Green dyadic method, to obtain qualitative estimates for the intensity enhancement and to discuss its relation to the observed spectral characteristics of the TPI-PL. According to the theoretical formulation of photolumines-

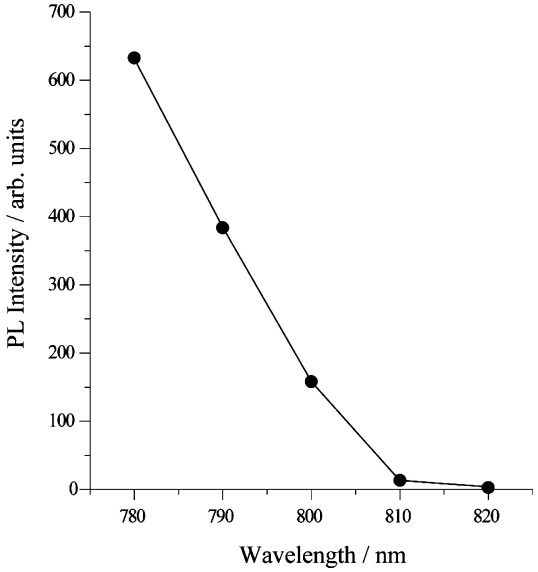

Figure 9. Excitation wavelength dependence of PL intensity from a single gold nanorod (25 ± 5 nm × 520 ± 50 nm). The PL ranging from 450 to 650 nm in wavelength was detected, and the incident field was polarized parallel to the long axis of the nanorod. Polarization of the PL was not specified.

cence from the surfaces of metallic films, TPI-PL intensity is approximately given by[4,34]

$$I \sim [L(\omega_{inc})]^4[L(\omega_{PL})]^2 \equiv \eta \quad (5)$$

where $L(\omega_{inc})$ and $L(\omega_{PL})$ denote local field correction factors for incident and emitted photons, respectively. The $L(\omega)$ factor is strongly dependent on the surface roughness and the microscopic structures of the roughened surface. We assume that eq 5 is valid for the TPI-PL from single nanorods. Then, the intensity enhancement factor is given by η in eq 5 and is estimated by calculating $L(\omega_{inc})$ and $L(\omega_{PL})$ using the Green dyadic method.

D.1. Calculation of the Electric-Field Enhancement. In the actual experiment, the nanorod is illuminated by radiation through the aperture probe. However, such a system is too complicated for a numerical electric-field calculation. To simplify the treatment and to obtain qualitative estimates of the enhancement factor, we do not consider a realistic measuring arrangement. Instead, we calculate the electric field near the rod, illuminated by a far-field radiation source. We consider a gold nanorod with a diameter of 20 nm and a length of 360 nm as a representative example. Such a nanorod shows a local plasmon resonance at a wavelength of ~790 nm, which is close to the present experimental excitation wavelength.

The total electric field, $\vec{E}(\vec{r})$, can be evaluated by utilizing the Green dyadic, $\vec{\vec{G}}(\vec{r},\vec{r},\omega)$, as the following Lippmann−Schwinger expression.[10]

$$\vec{E}(\vec{r}) = \vec{E}_0(\vec{r}) + k^2 \int_\Omega d\vec{r}' \vec{\vec{G}}_0(\vec{r},\vec{r}',\omega)[\epsilon_0(\vec{r}) - \epsilon_s(\vec{r}',\omega)]\cdot\vec{E}(\vec{r}') \quad (6)$$

where Ω is the volume of the nanorod. The focused electric field, $\vec{E}_0(\vec{r})$, described by Török and co-workers[35,36] was used as an incident field. The incident light was assumed to be linearly polarized along the long axis of the nanorod. The spot size of the incident light (wavelength ~780 nm) at the focal point was calculated to be ~500 nm (fwhm). The optical intensity at a position near the rod is defined as a local average of the intensity

$$I(\omega) = \int_S |\vec{E}(\vec{r},\omega)|^2 \, dS \quad (7)$$

where S is a small circular area parallel to the substrate located above the nanorod. The diameter of the circular area was chosen to be 50 nm considering the spatial resolution of the present experiment. The distance between the area, S, and the surface of the nanorod examined for the calculation was from 10 to 1 nm.

The incident intensity enhancement, $[L(\omega_{inc})]^2$, was calculated to be from 27 to 130 when the distance from the rod surface was varied from 10 to 1 nm. Similar electric-field enhancements were reported for contacted gold nanoparticles (dimer).[37] Intensity enhancements for emitted photons, $[L(\omega_{PL})]^2$, from the X (around 650 nm) and L (around 550 nm) regions were from 4.4 to 16 and from 1.7 to 4.4, respectively. As a result, the total intensity enhancement, $\eta = [L(\omega_{inc})]^4[L(\omega_{PL})]^2$, is ranging from 3.2×10^3 to 2.7×10^5. It is found from the present calculation that the electric-field enhancement due to the plasmon resonance of the nanorod seems to be quite effective. This strong enhancement may be an essential factor which causes the prominent TPI-PL from gold nanorods being observed.

D.2. The Spectral Feature of the PL. By collecting PL spectral data for many gold nanorods, it has been found that the observed ratio, $R = I_X/I_L$, of the integrated intensities of the two spectral components, I_X and I_L, ranges from 0.5 to 2, and mostly $R > 1$. On the contrary, the PL intensity ratio for the metallic film excited at 354 nm, which is comparable to the two-photon excitation energy of the present study, was reported to be $R \sim 0.12$.[4] It is obvious that the observed intensity ratio in the case of the TPI-PL for gold nanorods is larger than that for the metallic film. (Note that the PL spectrum in Figure 2 was corrected for the instrumental spectral sensitivity by a standard halogen lamp.) The difference between the PL spectra for the nanorod and the metallic film may be explained in terms of the field enhancements due to outgoing, ω_{PL}, photons. As discussed above, the enhancement, $[L(\omega_{PL})]^2$, for the X region is 2−4 times stronger than that for the L region in the case of nanorods. This is because the nanorod has a strong resonance due to the longitudinal plasmon mode in the longer wavelength.[33] Since the PL from the X region appears in the longer wavelength, it gains the intensity in resonance with the plasmon mode. In the case of a metallic film, on the other hand, such a resonance enhancement by the longitudinal plasmon mode is not expected.

To summarize, the relatively strong PL for the X region in the nanorod originates probably in the plasmon resonance, which is strongly dependent on the shape of the metal particle.

Conclusion

We have investigated two-photon-induced photoluminescence properties from various single gold nanorods by spectral, lifetime, and polarization measurements with an apertured scanning near-field optical microscope. In the PL spectra, we found two distinct peaks. The two peaks were attributed to PL arising from the electron−hole recombination near the X and L symmetry points. The very long (nanosecond) lifetime of the TPI-PL was found. The slow decay time was observed probably because the electrons located close to the Fermi surface were responsible for the observed PL process.

The excitation polarization dependence of the PL was studied, and a strong propensity was found. It showed a $\cos^2 \theta$

dependence against the angle of the incident polarization, and the TPI-PL was effectively excited by an excitation field parallel to the nanorod long axis. This result indicates that the TPI-PL proceeds through the sequential two-photon absorption. The polarization characteristics of the PL from the *X* and *L* regions were also investigated. Nearly perfect and partial polarizations, respectively, were found for the PL transitions from the *X* and *L* regions. These observations can be understood on the basis of the crystalline structure of the gold nanorod and the proposed PL mechanism.

In the TPI-PL images of single gold nanorods, we found peculiar oscillating patterns in the nanorods. We attributed the oscillating features to the spatial characteristics of the wave functions of the plasmon modes. The images correspond well with the LDOS maps of the nanorods calculated with the aid of the Green dyadic method. We also observed prominent wavelength dependence of the PL intensity inconsistent with the resonance character of the plasmon modes.

Acknowledgment. The work described herein is supported by Grants-in-Aid for Scientific Research (16350015, 16750017) from Japan Society for the Promotion of Science.

References and Notes

(1) Kreibig, U.; Vollmer, M. *Optical Properties of Metal Clusters*; Springer: Berlin, 1995.
(2) (a) Michaels, A. M.; Jiang, J.; Brus, L. *J. Phys. Chem. B* **2000**, *104*, 11965. (b) Xu, H.; Käll, M. *Phys. Rev. Lett.* **2004**, *89*, 246802.
(3) (a) Otto, A. *Surf. Sci.* **1978**, *85*, L392−L396. (b) Heritage, P.; Bergman, J. G.; Pinczuk, A.; Worlock, J. M. *Chem. Phys. Lett.* **1979**, *67*, 229.
(4) Boyd, G. T.; Yu, Z. H.; Shen, Y. R. *Phys. Rev. B* **1986**, *33*, 7923.
(5) Wilcoxon, J. P.; Martin, J. E.; Parsapour, F.; Wiedenman, B.; Kelley, D. F. *J. Chem. Phys.* **1998**, *108*, 9137.
(6) Mohamed, M. B.; Volkov, V.; Link, S.; El-Sayed, M. A. *Chem. Phys. Lett.* **2000**, *317*, 517.
(7) Imura, K.; Nagahara, T.; Okamoto, H. *J. Am. Chem. Soc.* **2004**, *126*, 12730.
(8) Busbee, B. D.; Obare, S. O.; Murphy, C. J. *Adv. Mater.* **2003**, *15*, 414.
(9) Nagahara, T.; Imura, K.; Okamoto, H. *Chem. Phys. Lett.* **2003**, *381*, 368.
(10) Girard. C.; Dereux, A. *Rep. Prog. Phys.* **1996**, *59*, 657.
(11) Greffet, J.-J.; Carminati, R. *Prog. Surf. Sci.* **1997**, *56*, 133.
(12) Economou, E. N. *Green's Function in Quantum Physics*; Springer-Verlag: Berlin, 1983.
(13) Morse, P. M.; Feshbash, H. *Methods of Theoretical Physics*; McGraw-Hill: New York, 1953.
(14) Yaghjian, A. D. *Proc. IEEE* **1980**, *68*, 248.
(15) (a) Rosei, R. *Phys. Rev. B* **1974**, *10*, 474. (b) Guerrrisi, M.; Rosei, R.; Winsemius, P. *Phys. Rev. B* **1975**, *12*, 557.
(16) Imura, K.; Nagahara, T.; Okamoto, H. *J. Phys. Chem. B* **2004**, *108*, 16344.
(17) Hodak, J. H.; Henglein, A.; Hartland, G. V. *J. Phys. Chem. B* **2000**, *104*, 9954.
(18) Link, S.; Burda, C.; Wang, Z. L.; El-Sayed, M. A. *J. Chem. Phys.* **1999**, *111*, 1255.
(19) Link, S.; Burda, C.; Mohamed, M. B.; Nikoobakht, B.; El-Sayed, M. A. *Phys. Rev. B* **2000**, *61*, 6086.
(20) Sun, C. K.; Valée, F.; Acioli, L. H.; Ippen, E. P.; Fujimoto, J. G. *Phys. Rev. B* **1994**, *50*, 15337.
(21) Varnavski, O.; Ispasoiu, R. G.; Balogh, L.; Tomalia, D.; Goodson, T., III. *J. Chem. Phys.* **2001**, *114*, 1962.
(22) Varnavski, O. P.; Mohamed, M. B.; El-Sayed, M. A.; Goodson, T., III. *J. Phys. Chem. B* **2003**, *107*, 3101.
(23) Kittel, C. *Introduction to Solid State Physics*; John Wiley & Sons: New York, 1986.
(24) Del Fatti, N.; Voisin, C.; Achermann, M.; Tzortzakis, S.; Christofilos, D.; Vallée, F. *Phys. Rev. B* **2000**, *61*, 16956.
(25) Link, S.; Wang, Z. L.; El-Sayed, M. A. *J. Phys. Chem. B* **2000**, *104*, 7867.
(26) Wang, Z. L.; Mohamed, M. B.; El-Sayed, M. A. *Surf. Sci.* **1999**, *440*, L809.
(27) Gai, P. L.; Harmer, M. A. *Nano Lett.* **2002**, *2*, 771.
(28) Bouckaert, L. P.; Smoluchowski, R.; Wigner, E. *Phys. Rev.* **1936**, *50*, 58.
(29) Ehrenreich, H.; Philipp, H. R. *Phys. Rev.* **1962**, *128*, 1622.
(30) Jones, H. *The Theory of Brillouin Zones and Electronic States in Crystals*; North-Holland: Amsterdam, The Netherlands, 1975.
(31) Weeber, J.-C.; Dereux, A.; Girard, C.; Krenn, J. R.; Goudonnet, J.-P. *Phys. Rev. B* **1999**, *60*, 9061.
(32) Matsuda, K.; Saiki, T.; Nomura, S.; Mihara, M.; Aoyagi, Y.; Nair, S.; Takagahara, T. *Phys. Rev. Lett.* **2003**, *91*, 177401.
(33) Imura, K.; Nagahara, T.; Okamoto, H. *J. Chem. Phys.* **2005**, *122*, 154701.
(34) Chen, C. K.; de Castro, A. R. B.; Shen, A. R. *Phys. Rev. Lett.* **1981**, *46*, 145.
(35) Török, P.; Varga, V.; Laczik, Z.; Booker, G. R. *J. Opt. Soc. Am. A* **1995**, *12*, 325.
(36) Török, P.; Varga, V.; Booker, G. R. *J. Opt. Soc. Am. A* **1995**, *12*, 2136.
(37) Bouhelier, A.; Beversluis, M. R.; Novotny, L. *Appl. Phys. Lett.* **2003**, *83*, 5041.